Absolute absorption cross section of 2-EHN in IR region

E-L Zins, M. Guinet, Delphy Rodriguez, Sébastien Payan

Absolute Absorption Cross section of 2-EHN in IR Region

E-L.Zins [a], M.Guinet*[,a], D.Rodriguez[b], S.Payan[b].

[a] Sorbonne Université, CNRS, MONARIS, UMR 8233, 75005 Paris, France.

[b] Laboratoire LATMOS, Laboratoire Atmosphères Milieux Observations Spatiales, Centre National de la Recherche Scientifique, Sorbonne Université, Université de Versailles-Saint-Quentin-en-Yvelines, F-75252 Paris, France

* Corresponding Author: mickael.guinet@sorbonne-universite.fr

Abstract

This paper presents the first determination of the absolute absorption cross section of 2-EHN from 850 to 3000 cm^{-1}. The domain of application of our measurement and its accuracy are discussed. DFT calculations were used for band attributions and the identification of the different isomers existing at room temperature.

The cross section measurements were used to study the adsorption/desorption processes of the gas that can occur on stainless steel cell walls and the evolution of this equilibrium when introducing 1 atm. of dry air. We also discuss the error made by neglecting those effects in terms of quantitative chemistry and air-broadening measurement.

Keywords

Absorption cross section, cetane improver, air pollutant, chemometrics, adsorption process, in-situ probing

Highlights

* 2-EHN absorption cross sections are retrieved within the 850 and 3000 cm^{-1} range

* DFT calculations were used as guidance for vibrational attributions, and several isomers were identified.

* Chemometrics multivariate linear regression (MLR) was propose a model for the estimation of 2-EHN partial pressure

* The adsorption/desorption equilibrium on the cell walls were in situ probed and estimated to be close to 52 %

Introduction

The chemical industry and chemical processes of the 21st century should respect the pillars of green chemistry. In particular, the concentration of entropic pollutants should be monitored in near real-time. It is important to be able to qualitatively and quantitatively identify the accidental release of different constituents, and to document individual exposure. A major source of anthropogenic air pollutants is still linked to road traffic. In addition to fuel oil, diesel contains additives to facilitate the combustion reaction: these are species whose exothermic decomposition makes it possible to lower the required temperature for starting the combustion process.

These constituents are called cetane improvers and the most common is 2-ethyl hexylnitrate (2-EHN).[1]-[4] Liquid at room temperature, it decomposes above 100°C. It then releases free radicals that contribute to reducing the engine's self-ignition time. 2-EHN is incorporated into fuels at a level of 0.3 to 1 g.L^{-1}, corresponding to a production of 105 tons worldwide.[5] Since it is used in very large quantities, it may be accidentally released into the atmosphere. This gas is involved in atmospheric chemistry [6, 7], and could cause secondary reactions. As a result of its exothermic decomposition, specific studies are required to characterize it. Furthermore, since 2-EHN is not easily biodegradable [8] and not soluble in water, it can cause long term pollution.[9]. While studies have already been carried out on its decomposition and characterization in the liquid phase,[10],[11],[12] only few studies have concentrated on the gas phase. FTIR is a widely used technique for atmospheric gas quantification. Pioneering studies have been carried out on 2-EHN, [13],[14],[15] but no data are available for the spectral signature of the vapors in the mid-IR domain. To complete and develop the previous studies, we propose here a thorough analysis of its IR spectrum in the gaseous phase. This precise analysis could allow its rapid identification near strong sources such as fuel stations and airports.

In a second step, we propose different complementary approaches for the quantitative analysis in the gas phase based on a chemometric method. Indeed all the studies mentioned above [10-15] used the chemometric approach while atmospheric spectroscopy uses directly the absorption cross section data. Comparisons between the two complementary methods are therefore needed and useful. For an accurate quantification of a constituent by gas phase spectroscopy, it is essential to take into account the adsorption/desorption processes that can occur on the cell walls. We evaluate these effects and try to limit the biases due to exchange processes.

Material and Methods

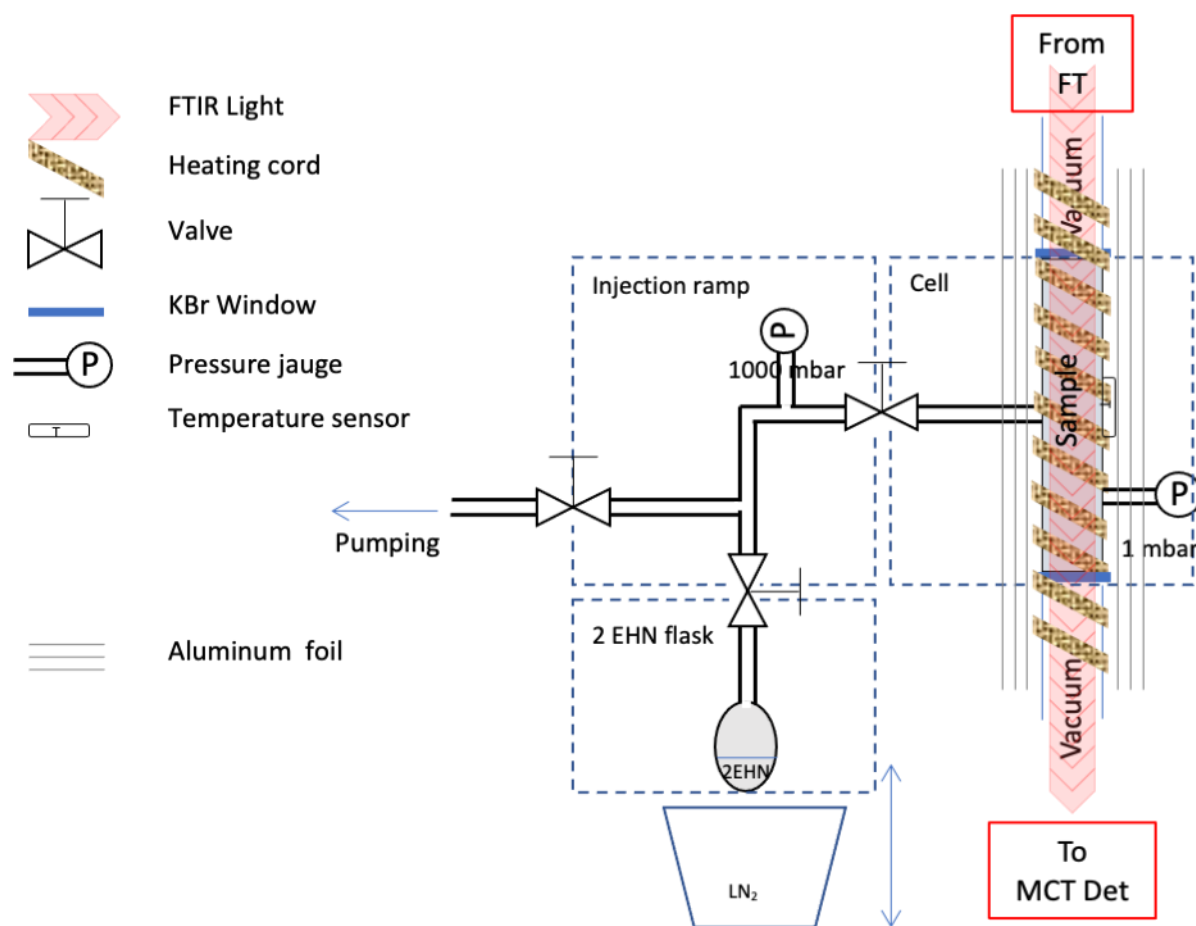### 1. Experimental setup

Fourier transform spectra have been recorded between room temperature and 318 K using the Bruker IFS 120 HR interferometer of MONARIS [16]. The resolution was set to 0.5 cm^{-1}. A 1.57 mm aperture radius of the iris in front of the Globar source has been chosen and the focal length equals 418 mm for all spectra. A scheme of the experimental setup is presented in Figure 1.

The gas sample is obtained by evaporation of liquid 2-EHN and the pressure is recorded with a capacitive gauge. We mostly used pure 2-EHN gas but some mixtures with dry air (100-1000 mbar) have also been used. 2-EHN has a low vapor pressure of 0.27 mbar at 20°C. Moreover, it is a polar gas that undergoes a strong adsorption on the cell walls. As a consequence, a stable pressure above 0.2 mbar is difficult to maintain over 15 min. In addition, the outgassing (or micro-leaks) rate of the cell is 0.03 mbar/hour. Therefore, we have chosen pressures between 0.02 and 0.2 mbar which allowed to control the purity of the gas.

The flask of 2-EHN is first frozen in LN_2 and pumped with a turbo-molecular pump allowing to evacuate non condensable gases (N_2, O_2).


Figure 1: Scheme of the experimental setup used for the present study. "MCT Det" and "LN2" stand for "MCT Detector", "Liquid Nitrogen", respectively.

The gas is then slowly warmed until 20°C while keeping the pumping to evacuate condensable gases that are more volatile than the 2-EHN. Then the cell and the entrance ramp are conditioned with

the chosen pressure during 10 minutes. After passivation we quickly pumped on the 2-EHN flask together with the cell and the injection ramp to not destroy the fragile passivation layer made on stainless steel surface. Therafter, the pumping is stopped and the cell is closed when the pressure of "fresh" gas reaches the passivation pressure. This procedure is adapted to evacuate the non-condensable gases, but it is difficult to separate the 2-EHN from some residual condensable gases. A time of 45 seconds is needed to record one spectrum. During this time, the total pressure of 2-EHN evolve by less than 2%.

The commercial gas sample of 2-EHN was provided by Sigma Aldrich with a stated purity of 98.0% in natural abundance. The pressures of 2-EHN (ranging from 0.02 to 0.2 mbar table 1) inside the cell have been measured with a Baratron gauge with an accuracy better than 0.25% and the temperature of the gas sample has been determined with an accuracy of ± 0.1 K using a platinum resistance thermometer inside the cell. The device was pumped over the night. Before each day of measurement, an outgassing rate was measured and taken into account to correct the purity of the sample.

The average interferograms (co-addition of 20 scans) have been Fourier transformed using the procedure included in the Bruker software OPUS package. As illustrated in Figure 2, each average spectrum is divided by a "white spectrum" recorded before each set of measurements.
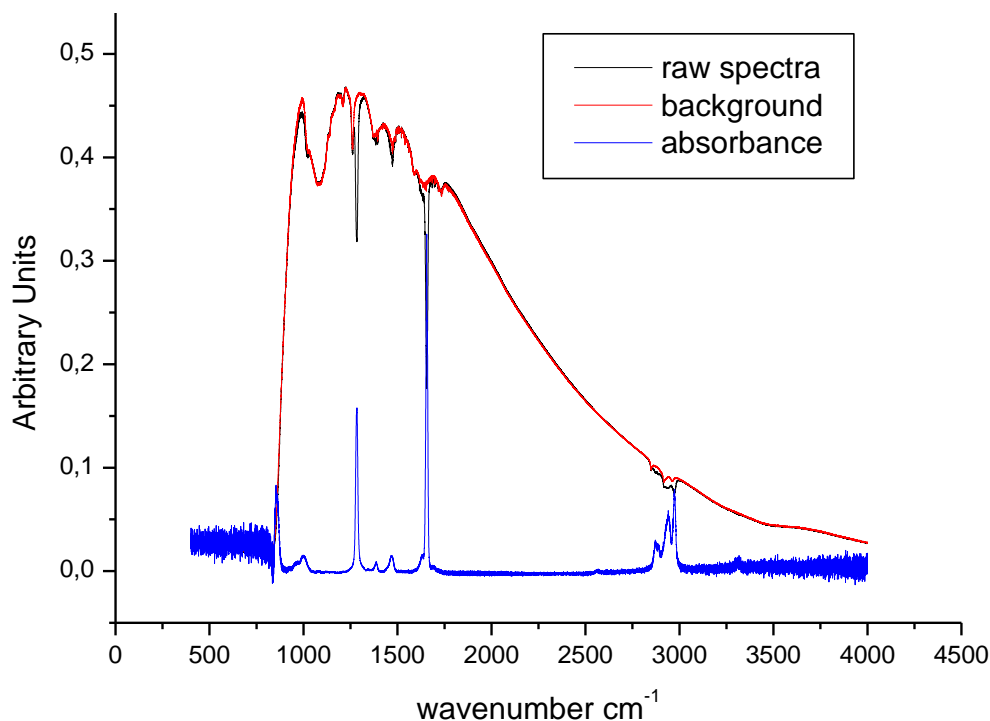
Figure 2: Generation of the absorbance spectrum from the background (I_0) and the raw spectrum (I).

The interferometer was equipped with a KBr beam splitter, a MCT photovoltaic detector, and a Globar source. Two stainless steel cells of 68.8 cm and 31.8 cm path length were used. Those cells were both equipped with KBr windows. A Platinum thermometer (Pt100) was inserted into the cell to probe the gas temperature directly. The cell is surrounded by a heating cord, and 3 aluminum layers to ensure a good thermal homogeneity.

Spectrum number	Pressure (mbar)	Temperature (°C)	Path length of the cell (cm)
1	0.025	24.4	31.8
2	0.027	24.4	31.8
3	0.033	25.9	68.8
4	0.053	25.6	68.8
5	0.098	24.3	68.8
6	0.101	24.6	68.8
7	0.102	24.8	68.8
8	0.103	24.8	68.8
9	0.133	24.1	31.8
10	0.181	25.6	68.8

Table 1: Experimental conditions for the IR spectra (20 scans for each spectrum) of gaseous 2-EHN that were considered in the present study

2. Qualitative analysis - Identification of the vibrational modes

For this molecule, different isomers may exist depending on the relative position of the carbon chains and the nitrate group. In order to allow for a reliable identification of the compound, it is first necessary to characterize its IR spectrum. In the absence of high-resolution or noble gas matrix spectra, we have made theoretical calculations. These were performed with the Gaussian09 software. [17]

The aim of this part of our work was to identify the main isomers that may exist at room temperature. For this purpose, a two-step procedure was applied, starting with a search for the different isomers in DFT, followed by a vibrational characterization. More precisely, the PBE1PBE functional was selected, with the 6-31+G(d,p) basis set, using the additional keywords scf=(Tight,MaxCycle=500) and Int=UltraFine.

3. Quantitative analysis - Assessment of the dataset quality

For the quantitative analysis, data have been evaluated following two approaches.

The first method takes advantage of the absorption cross sections at a given wavenumber or over a small spectral domain (area under the curve) being proportional to the partial pressure of the active molecule. This approach is very simple and allows to evaluating the limits of the data set. It is particularly adapted for sources a like laser diode, a led, or a vapor lamp. However, this approach can't be used if another gas is present and affects the IR bands in the chosen wavenumber range of the analysis. In this case a broadband instrument recording a large wavenumber area is needed and a different method which is robust against interfering gases must be used. We have employed chemometric approach, which has the advantage of being based on freely available and easy-to-use software.

The data processing was done as follows:

i. Firstly, a FORTRAN program was used to extract the absorption at a fixed wavenumber and to use it for quantitative analysis. The choice of a specific and representative wavenumber is crucial here to limit the error that may be induced by pollutants. The FORTRAN program used in this study is provided as Supplementary Material.

ii. As the presence of a molecule in a complex mixture (such as polluted air under atmospheric conditions) requires a spectrum over a wide spectral range, we have also employed a chemometric approach for the calibration. More precisely, a multivariate linear regression (MLR) study was performed using seven selected wavenumbers in the spectrum. It is worth mentioning that since 10
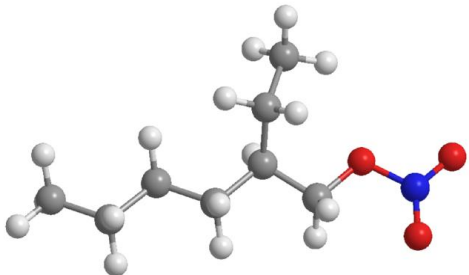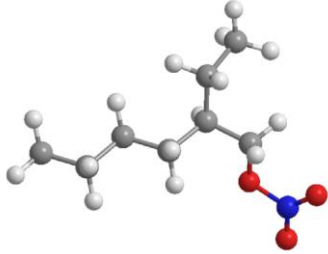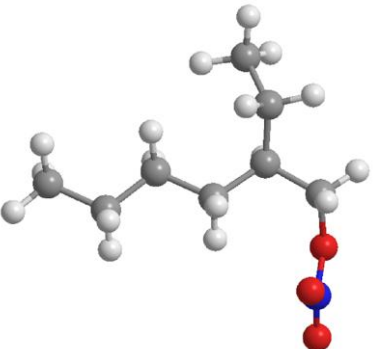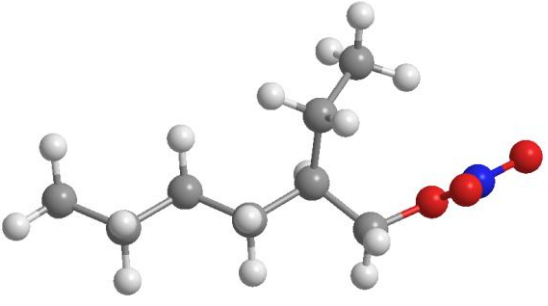
spectra were used for the calibration, the maximum value of independant and characteristic wavenumbers is 9. Before carrying out this study, it was checked that the quality of our spectra did not require any pre-treatment (no baseline deviation, no shift of the spectra with respect to each other, no improvement after SNV treatment). Then, a representative set of wavenumbers spread all over the spectral range and for which the nature of the vibration could be identified, was chosen. In these statistical analyses, the set of n spectra is treated as a matrix of n rows, each column corresponding to a wavenumber. This matrix is then used to handle the noise and then to perform a supervised quantitative analysis. A supervised analysis is one in which a data set is used to build a predictive model. This is the case for the calculation of a calibration curve. Following Beer-Lambert's law, it is quite natural in this case to choose a linear regression. Rather than using a single wavenumber as a basis for the model, we preferred to use a multiple linear regression model, based on the simultaneous absorbance values measured at seven given wavenumbers, to increase the robustness of the analysis. This analysis was carried out using the ChemFlow software [18]."

Results and discussion.

1. Characterization of the isolated molecule

a. Theoretical characterization of each isomer

Due to free rotations around simple bonds, different rotamers of 2-EHN are likely to exist at room temperature. The influence of these isomers on the vibration spectrum has been evaluated using quantum chemistry calculations. Table 2 presents some examples of structures (A,B,C,D,E) very close in energy ($\Delta E < 12$ kJ/mol) that were identified. The IR spectrum observed at ambient pressure and temperature will therefore be the convolution of the spectra of these different isomers. All these isomers will contribute to the registered IR spectrum.

A $\Delta E = 4.5$ kJ/mol	B $\Delta E = 0$ kJ/mol
Sum of electronic and ZPE : -594.49497 Hartree	Sum of electronic and ZPE : -594.49669 Hartree
C $\Delta E = 11.7$ kJ/mol	D $\Delta E = 10.9$ kJ/mol
Sum of electronic and ZPE : -594.492244 Hartree	Sum of electronic and ZPE : -594.492557 Hartree

| E | ΔE = 6.0 kJ/mol |
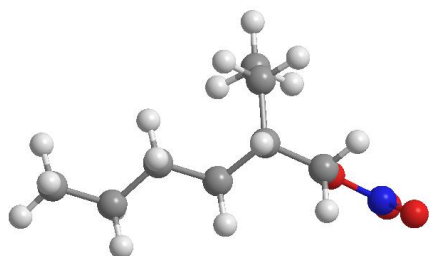
Sum of electronic and ZPE : -594.494373 Hartree

Table 2: Some stable structures obtained for the 2-EHN with their energetics.

The Cartesian coordinates as well as the vibration frequencies calculated for these isomers are presented as Supporting Information. Table 3 shows the calculated wavenumbers as well as associated theoretical intensities and their attributions for the most stable isomers, A and B.

Isomer A		Attribution	Isomer B	
Wavenumber (cm^{-1})	Theoretical intensity		Wavenumber (cm^{-1})	Theoretical intensity
1785	428	N-O twisting	1785	429.0552
926	173	N-O stretching linked to the carbon chain		
931	132		934	240
1368	126	H methyl wagging, N-O sym stretching	1366	111
1434	108		1432	110
1385	61		1385	63
1050	13	C-O asymm stretching		
1036	57		1043	58
1068	21	C-O asymm stretching	1061	41
1068	17			

		H methyl wagging, N-O sym stretching	1338	34
792.9368	12	NO_3 umbrella mode	793	12

Table 3: Theoretical IR characterization of the two most stable isomers of the 2-EHN (isomers A and B in Table 2)

For the identification in the atmosphere, the target bands must be located within the spectral range accessible for atmospheric remote sensing as provided by meteorological satellites, such as IASI [19]. It thus appears that for a qualitative analysis of 2-EHN in real samples of polluted air (determination of the presence or absence of this pollutant), it is relevant to focus on the vibrations associated with the NO_3 group, which will be more characteristic than those associated with carbon chains. This is demonstrated in the Figure 3.
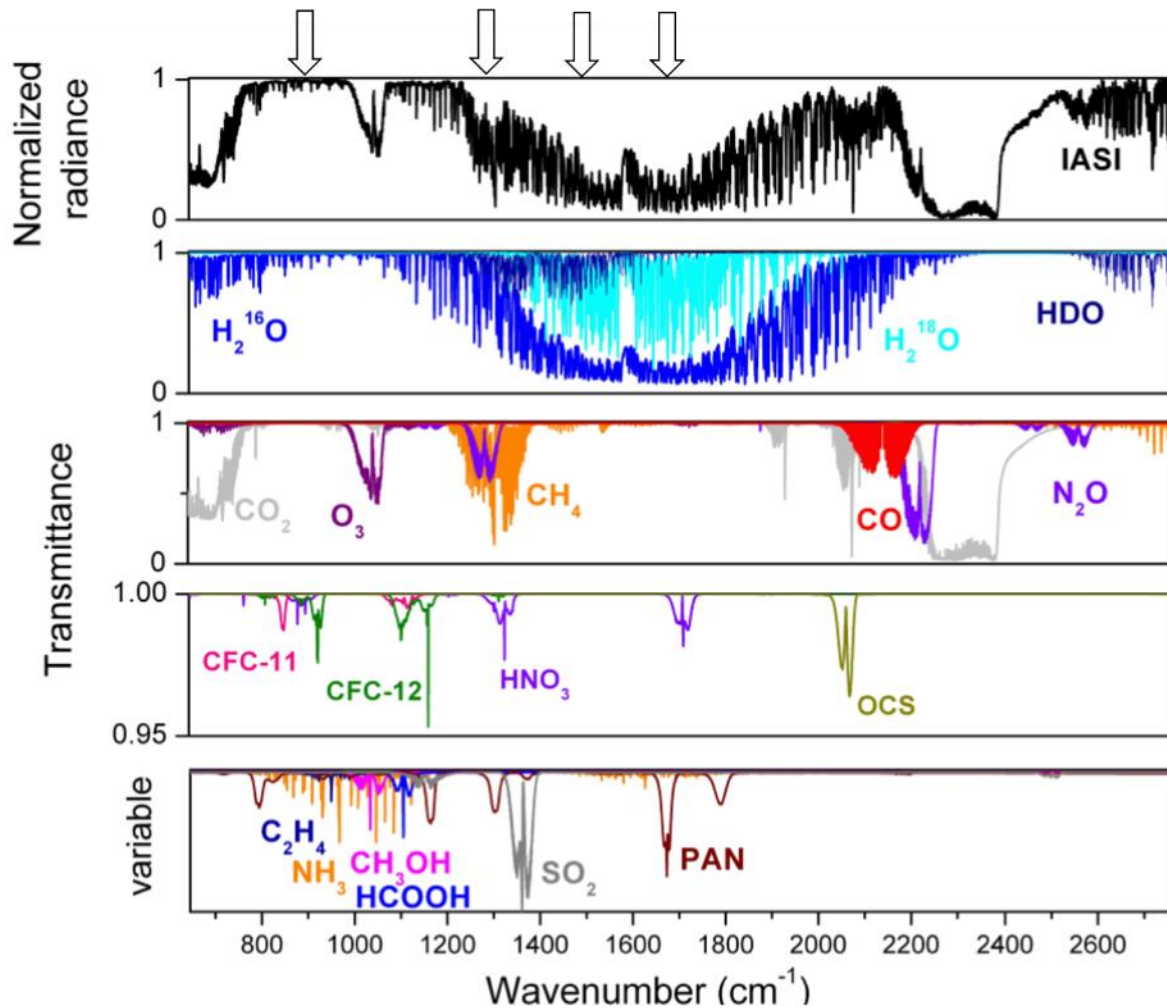
The calculated frequencies further show that the spectra of both isomers are too close to be experimentally separated. Indeed, the strongest bands differ by only a few cm^{-1}, with the notable exception of the band at 1338 cm-1, that appears to be characteristic of the B-isomer.

b. Experimental spectra and assignment of the vibration modes

The average absorption cross section (absorbance/pressure/length at a given wavenumber) is obtained by the averaging of 10 spectra (Figure 4). All these data are presented as Supplementary Information in the form of a table containing the absorption as a function of wavenumber. This formatting is directly applicable to evaluate absorption measurements at a single wavenumber or the complete data set can be integrated into a radiative transfer code. The molecular signal presents multiple absorption areas; each of them has a complex form that may be due to the coexistence of multiple isomers, as given in Table 2 and Table 3. Table 4 shows the attribution of the experimentally observed vibrations.
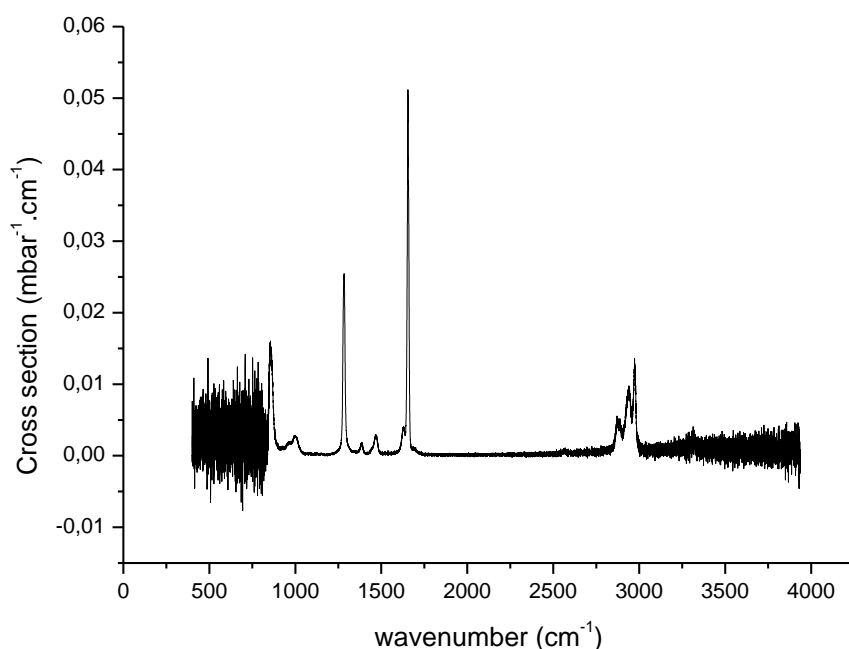
Figure 4: average absorption cross section of 2-EHN (obtained as average of 10 spectra)

12

Experimental Wavenumber (cm^{-1})	Tentative attribution	Calculated wavenumber of the main isomer (cm^{-1})
855	NO$_3$ umbrella mode	792
	N-O stretching linked to the carbon chain	926; 931; 934
990	N-O stretching linked to the carbon chain	926; 931; 934
	C-O asymm stretching	1036; 1043; 1048
1280	H methyl wagging, N-O sym stretching	1338; 1366; 1368; 1385
1385		
1470	H methyl wagging, N-O sym stretching	1432; 1433
1630	N-O twisting	1784
1655		
2870	C-H symm stretching of the CH$_2$ linked to the NO$_3$ group	3048; 3077
2890		
2940		
2975		

Table 4: Tentative attribution of the experimentally observed vibrations based on the comparison with the calculated wavenumbers for the most stable isomer of the 2-EHN (isomer A in Table 2)

2. Study of the evolution of absorbance as a function of pressure

In order to be able to quantify traces of 2-EHN in complex samples, it is necessary to consider different calibration techniques, which can be used depending on the measurement conditions. For this study, ten spectra recorded using two different cells to cover a representative range of gas concentrations, were selected. We particularly focused on characterizing samples corresponding to low pressures of 2-EHN that are likely to be encountered in real samples of polluted air.

i. Calibration using the absorbance at 1283 cm^{-1}

With respect to applications in atmospheric spectroscopy, it is interesting to be able to quantify species from a very restricted spectral area, or even on a single band, for which the spectra would be simple and quick to record routinely. These approaches are also relevant in the case of using spectrometers with laser diodes. To determine whether such an approach could be used in the present case, we selected the absorbance at the label 1283.7980425006 cm^{-1} in the spectra file, and perform a calibration. The linear regression obtained using this calibration, as well as the random distribution of the residuals (Figure 5) show that this approach is quite relevant. However, for the study of complex samples in which the 2-EHN may be present in trace amounts (polluted air), it seemed necessary to develop calibrations based on the study of a wider spectral range. The affine function obtained in Figure 5 reflects the Beer-Lambert's law and the dispersion around this law is a good approximation of the reproducibility of our measurements. The final uncertainty can be calculated as the square root of the quadratic sum of the different systematic errors (temperature, pressure, commercial purity, pressure variation during the recording, path length…) and of the measurement reproducibility. All those contributions lead to an accuracy of 9 %.
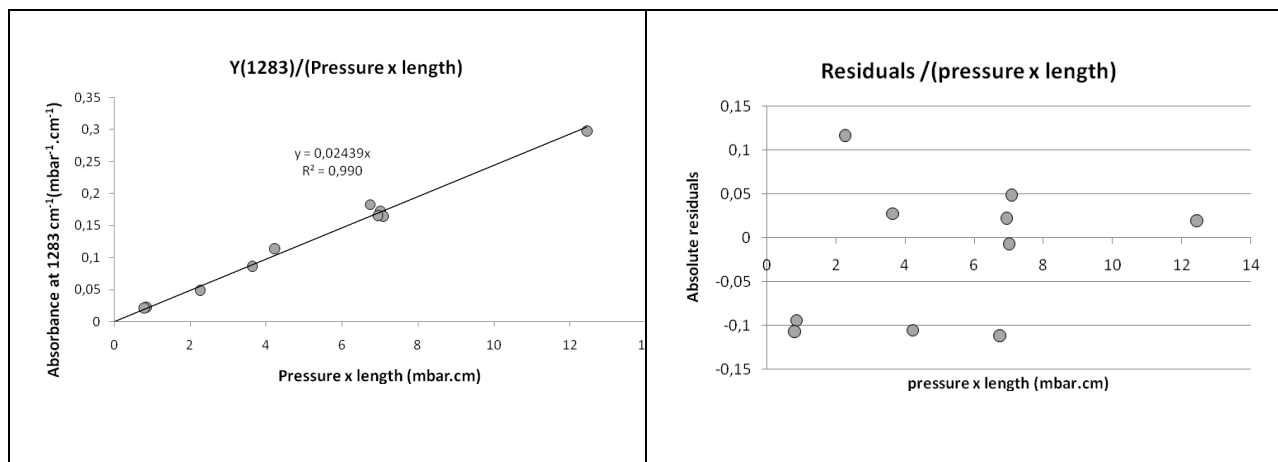

Figure 5: Y(1283.8) as a function of the pressure x length (left) and difference between the affine function and Y(1283) (right)

ii.   Calibration using chemometric approach

For these samples, seven wavenumbers covering the entire mid-IR range considered. The intensity at each selected wavenumber for each of the samples is indicated in table 5.

λ (cm⁻¹) P × L of 2-EHN (mbar.cm)	850.0531	865.0791	1000.072	1290.065	1460.011	1638.073	1660.01
0.80	0.014	0.012	0.001	0.010	0.001	0.002	0.028
0.86	0.013	0.016	0.005	0.014	0.004	0.005	0.033
2.27	0.021	0.023	0.006	0.025	0.004	0.005	0.067
3.65	0.043	0.040	0.008	0.041	0.005	0.006	0.113
4.23	0.047	0.047	0.010	0.051	0.010	0.020	0.136
6.74	0.100	0.095	0.020	0.088	0.015	0.021	0.240
6.95	0.071	0.074	0.017	0.080	0.013	0.016	0.219
7.02	0.070	0.065	0.014	0.081	0.011	0.014	0.225
7.09	0.081	0.077	0.017	0.079	0.012	0.014	0.216
12.45	0.141	0.135	0.025	0.136	0.016	0.028	0.380

Table 5: Presentation of the spectroscopic features of the samples selected for the chemometric analysis: absorbances (in a.u.) at the seven selected wavenumbers for ten spectra. For each registered spectrum, the corresponding partial pressure x lenght (P*L) is indicated in the first column.

The Multivariate Linear Regression method allows to find a linear relation between the concentration and the intensity of all these bands. It is worth mentioning cross sections at the seven chosen wavenumbers are simultaneously used for the linear regression. In the case of the analysis of complex mixtures, this approach is more applicable than the use of Beer-Lambert's law at just a single wavenumber, if the selected wavenumbers are correctly chosen with respect to the absoption bands of polluted compounds. Indeed, in complex mixtures such as a polluted air sample, other compounds may share absorption bands with those of 2-EHN. The simultaneous recording of seven characteristic spectral bands (without any C-H or C-C vibration, common to many pollutants) after having checked the intensity ratios of the selected bands, will avoid erroneous identification of 2-EHN. The random distribution of the residuals and the linear variation of the normal QQ plot suggest that the description is correct, and can be validated.

The random distribution of the residuals (Figure 6), the high value of R^2 (0.997, Figure 7) and the linearity observed on a large central part of the Q–Q (quantile-quantile) plot (Figure 8) suggest that the description is correct, and can be validated [20]. It should be mentioned that the deviation of the Q-Q plot on the extreme values is normal, and the higher contribution of the residuals for low values of partial pressure can be explained by a lower signal to noise ratio.

P × L of 2-EHN (mbar.cm)	Residuals
0.795	5.22E-04
0.859	4.65E-03
2.270	-6.83E-03
3.646	1.11E-03
6.742	-2.60E-04
6.949	-2.08E-03
7.018	1.71E-03
7.086	-1.61E-04
4.229	9.12E-04
12.453	4.25E-04
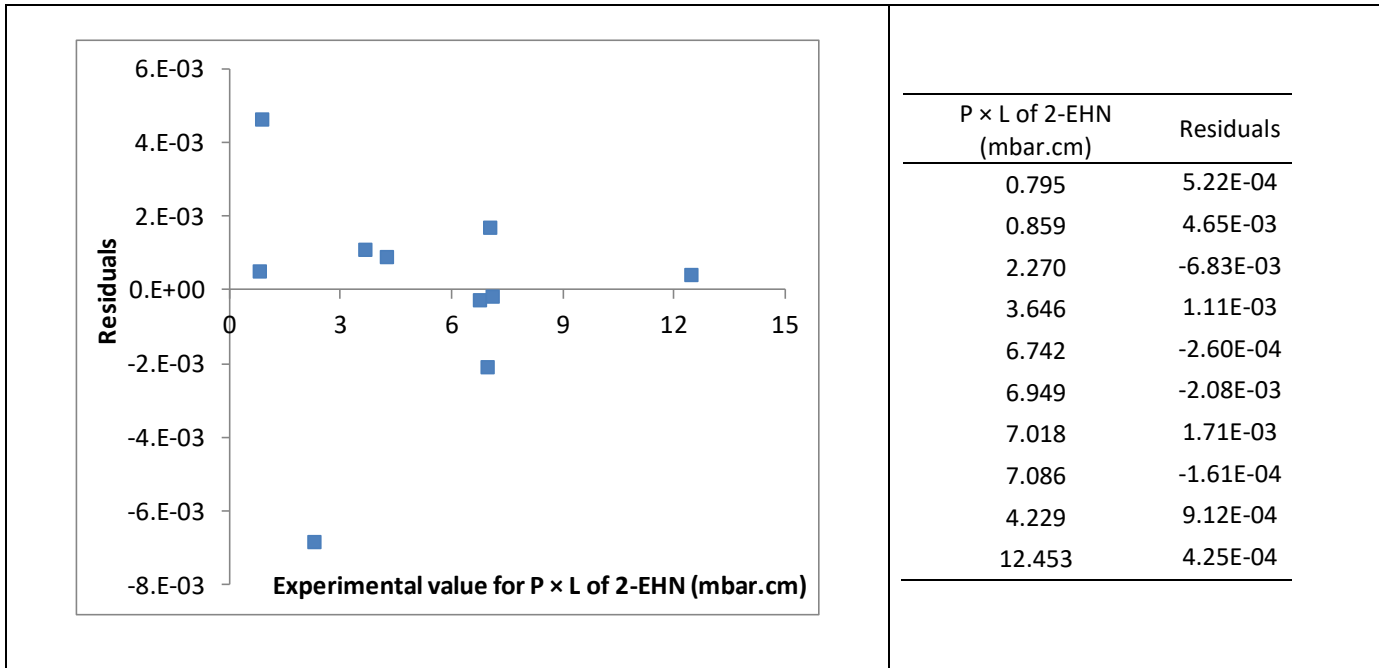
Figure 6: The random distribution of the residuals obtained after the chemometric treatment of the spectra presented in Table 5.

Experimental value for P × L of 2-EHN (mbar.cm)	Predicted value for P × L of 2-EHN(mbar.cm)
0.795	0.763
0.859	0.700
2.27	2.752
3.646	3.577
6.742	6.793
6.949	7.091
7.018	6.879
7.086	7.086
4.229	4.188
12.453	12.453
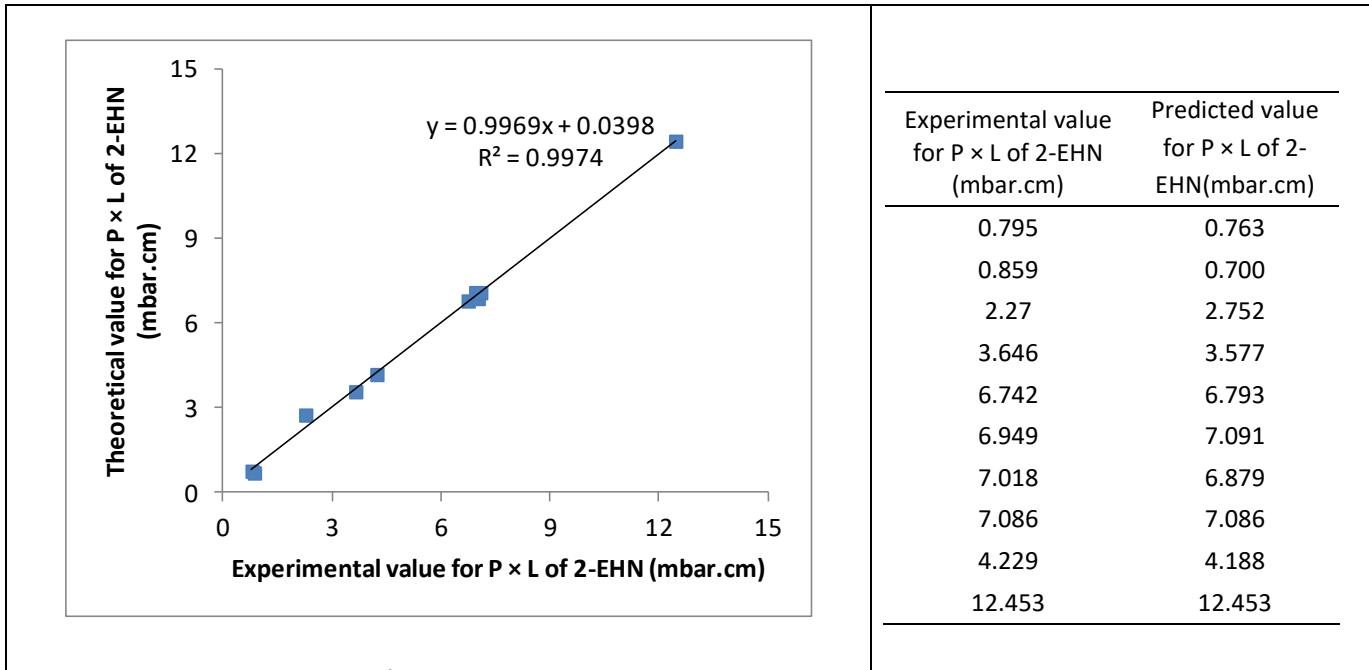
Figure 7: Determination of the R^2 value associated with the model. Comparison of predicted and measured pressures based on the chemometric analysis of the spectra presented in Table 1.
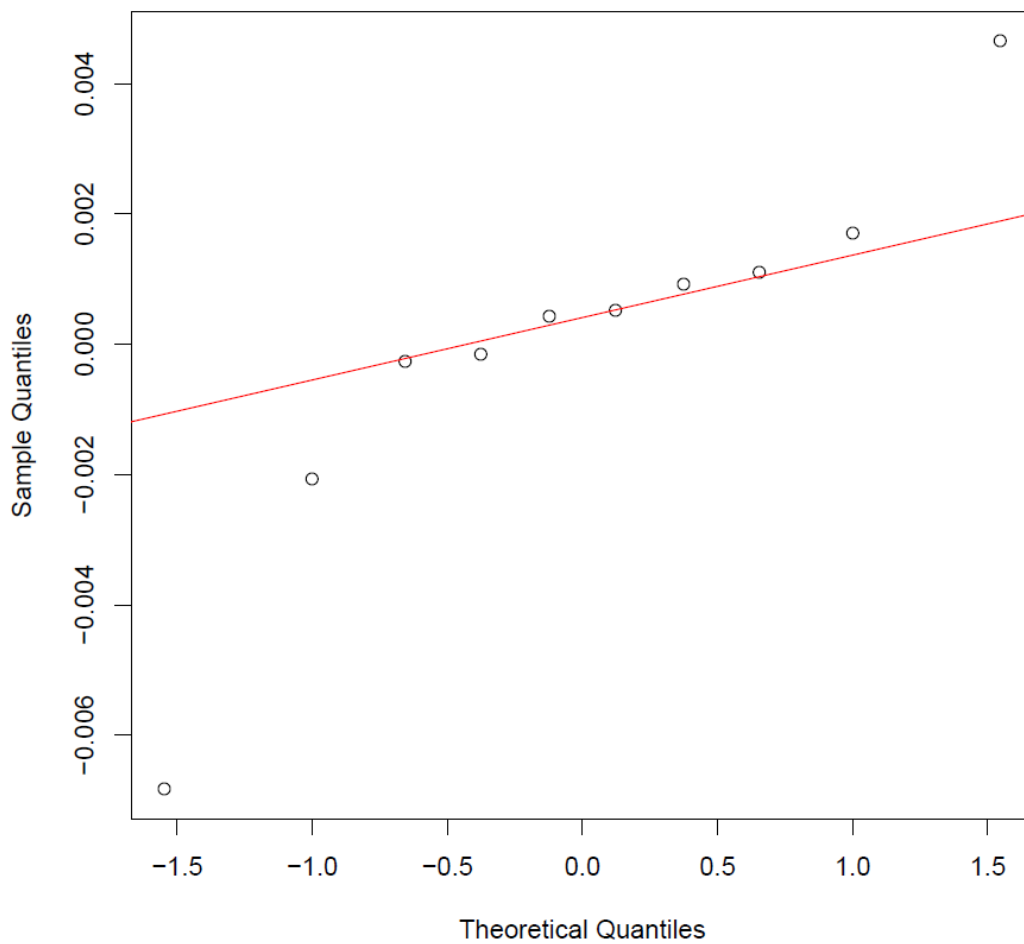
Figure 8: Q–Q (quantile-quantile) plot

By measuring the intensity at the selected seven wavenumbers, the unknown 2-EHN concentration of a sample could be deduced (Figure 8). However, in the case of polluted air samples, the choice of the wavenumbers is crucial and should be adapted to the nature of pollutants.

3. Influence of resolution and pressure

After this first characterization, the effects of pressure and spectral resolution have been investigated.
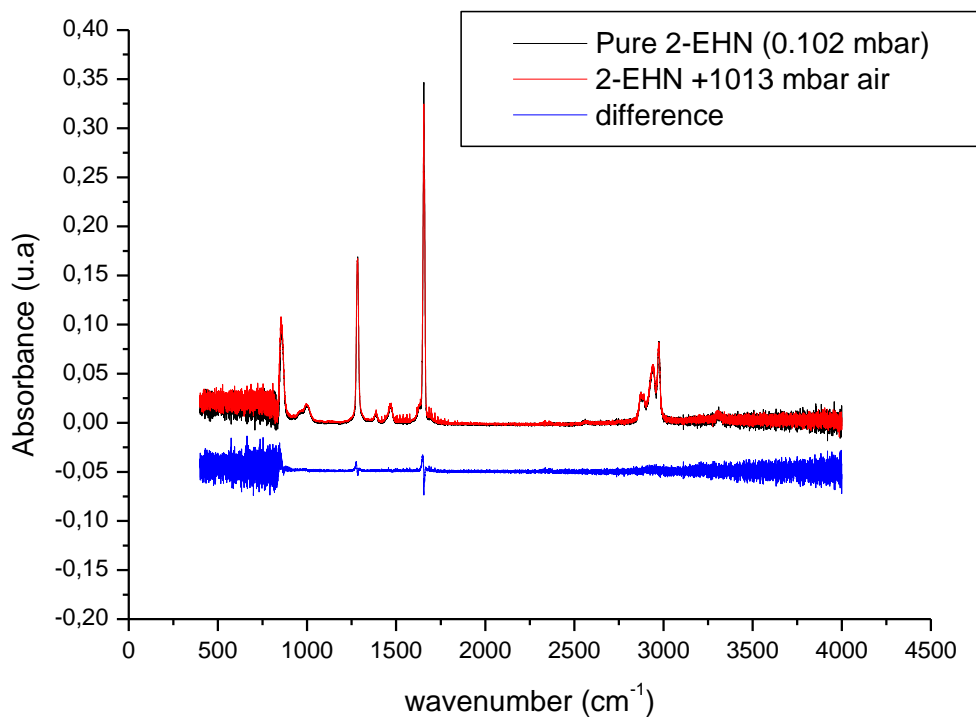
Figure 9: Comparison between a spectrum of pure 2-EHN and the same pressure of 2-EHN with 1013 mbar of air added

Figure 9 shows a pure spectrum of 2-EHN and a mixing of 2-EHN and air. As previously discussed, 2-EHN is a polar molecule and the introduction of air will affect the fragile layer of adsorbed molecules leading to an increase of 2-EHN in the cell. The spectrum of the mixing is arbitrarily re-scaled to help for the comparison. The difference between the two spectra shows that the shape of the spectrum is not dramatically affected due to the pressure: only a slight shift of the bands around 1250 and 1700 cm^{-1} is observed.

Due to the large mass of the molecule (175.23 $g.mol^{-1}$), the rotational spectra is not resolved leading to wide band of 50 cm^{-1}. This spectrum is convoluted with the apparatus function and air-broadened. The resolution of the FTIR is 0.5cm^{-1} and the air broadening is typically around 0.1 cm^{-1} atm^{-1}. As a consequence, the data set can be used on spectrometers of different resolution.

Figure 9 illustrates this fact. The difference between the pure sampling and the mixing with air is barely observable. A slight shifting is observed, but due to the difficulties of knowing the partial pressure in the mixture, it is preferable to record the spectra with pure 2-EHN and use for evaluation

18

even under atmospheric pressure conditions. By the same argumentation, our spectra can be used with a large set of resolutions.

Application, partial pressure in situ measurements

While capacitor gauges are accurate for the recording of total gas pressures, absolute absorption cross sections allow to perform an accurate in situ probing of the partial pressure of a target gas. Many applications monitor a trace amount of gas within a large amount of perturbing gas. We choose to add the perturber gas following a standard protocol [20,21] when measuring the spectroscopic broadening by air or by N_2.

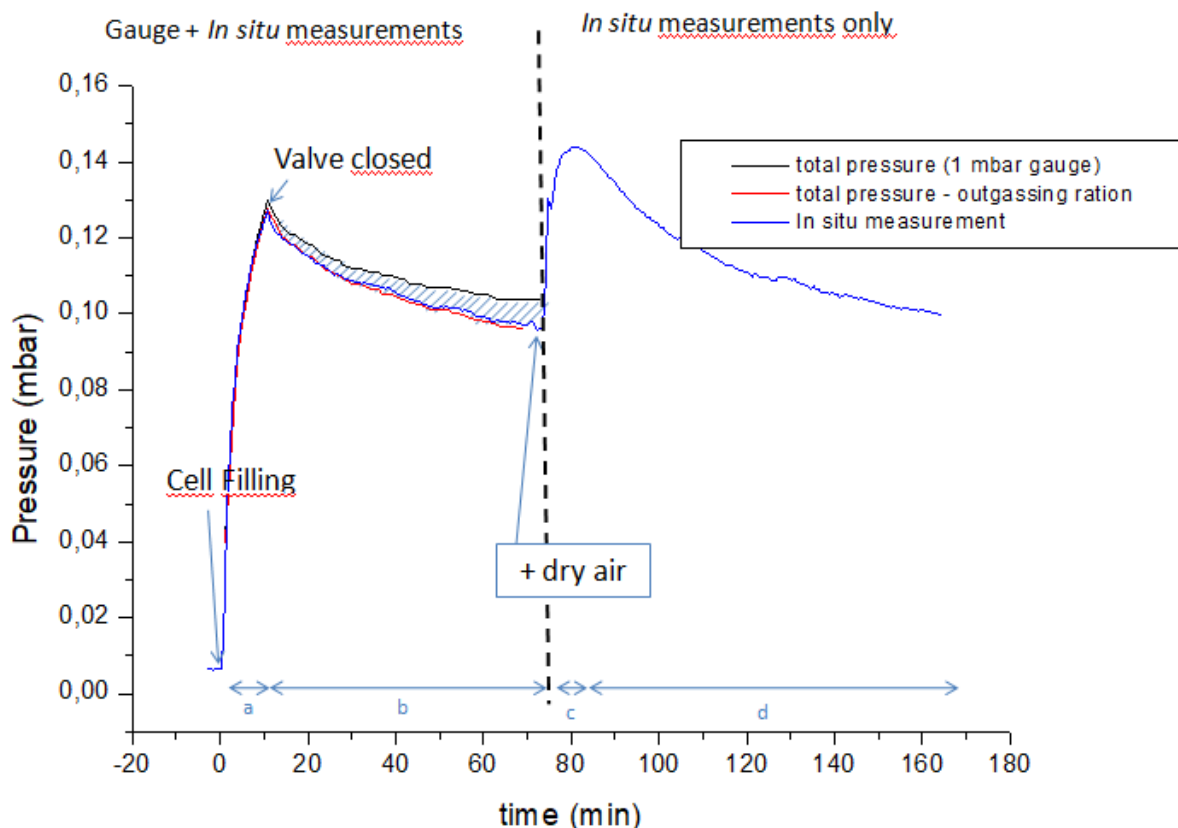
Figure 10: evolution of pressure both with pressure gauge and in situ spectroscopic probing. During the filling (a), the adsorption (b), the desorption due to the dry air (c) and the final adsorption (d)

In order to provide reliable quantitative evaluations, the calibration spectroscopic studies performed in the laboratory must be as accurate as possible. However, in the case of gas phase

analyses, it is known that there are important biases, which can dramatically distort the measurements, especially when the active gas is diluted in a large amount of perturber gas. For example, gas exchange with the walls interfere with the measurements whatever the precision of the spectrometeris, and the type of cell used. There are two types of phenomena that can occur:

- a desorption of residual molecules adsorbed on the walls, even in the case of the use of advanced pumping systems,
- and an adsorption on the walls of the compound to be analyzed.

This problem is well known and studied by the spectroscopists, but there is not so much detailed examples available on setups similar to those used by atmospheric spectroscopists. However this phenomenon depends both on the setup (pumping system, size and constitution of the cell ...), and on the molecule of interest (polar or non-polar ...). We wanted to estimate the order of magnitude of the possible bias that can be made in some studies when the adsorption effect is neglected. We are convinced that these adsorption/desorption phenomena on the walls lead to significant errors if they are not taken into account.

The first step is to record the outgassing rate of the residual gas, simply by closing the cell and measuring the total pressure increase. This outgassing rate is assumed to be the same with and without gas. To this end, we carried out a pumping as complete as possible, allowing the "ultimate" vacuum of the cell to be reached. Then the cell was "filled", with a precise amount of gas to be analyzed ("a" on Figure 10). After stopping the addition of gas, we follow the evolution (a priori an apparent decrease) of the partial pressure ("b" in Figure 10) of the compound of interest together with the total pressure. This step can be interpreted as the "sticking" on the walls of the gas of interest, and the desorption of residual gases (ie the degassing of the cell (hatched area in Figure 10)). After the addition of one atmosphere of dry air, the total pressure can only be measured by a 1000 mbar pressure gauge. In this case, the partial pressure of the target gas can only be probed by spectroscopy ("c" in Figure 10). Indeed, measurements of real samples, such as polluted air, will be carried out not only with the molecule of interest, but with the molecule of interest mixed with air. However, the presence of air can modify the equilibrium of the molecules adsorbed on the walls, which can modify the effective cross sections deduced from the experimental observations. More precisely, the addition of air can lead to the unsticking of molecules that were previously adsorbed on the walls of the cell (c

on the Figure9), leading to an artificial increase of the effective cross section deduced for the molecule of interest. Finally the molecules readsorb on the cell walls towards a new equilibrium ("d" on Figure 10).

In the present study, 0.13 mbar of 2-EHN was introduced into the cell of the spectrometer. This pressure was determined both by the pressure gauge (total pressure) and by using the previously performed calibration curve (partial pressure). This filling took 10 min. After closing the valve, a decrease in the pressure read by the pressure gauge was noted. This decrease lasts about 50 min, and corresponds to the adsorption of 2-EHN molecules on the cell walls. According to the pressure gauge, the pressure drop reaches 0.105 mbar. But according to the calibration curve, the partial pressure of 2-EHN is lower, at 0.0955 mbar. This difference corresponds to the outgassing rate measured in the emptied cell. After the addition of 1 mbar of air, the spectroscopic monitoring shows an increase of 52% in the partial pressure of 2-EHN. Note that the addition of dry air was performed using a different inlet than the one used for addition of 2-EHN and the common parts were well pumped. The increase of 2-EHN can be attributed to desorption from the cell walls. The effective partial pressure of 2-EHN deduced from the experimental observations just after the addition of dry air is 0.145 mbar. A return to a pressure close to the first equilibrium pressure reached before the addition of dry air is observed after about 50 min and does not seem to have reached the equilibrium Table 6 shows some examples of errors that can be made depending on the time lapse after initial filling.

So depending on when the actual measurement is made, the amount of 2-EHN varies between less than 0.1 mbar and 0.145 mbar. For spectroscopic broadening measurements, for example, the average partial pressure should be adjusted, but its complicated time evolution should still lead to some residual error. For some quantitative chemistry applications the measurement of the initial amount is also not accurate enough and in situ monitoring is an advantage.

	GM (mbar)	ISM (mbar)	Time (min)	Possible Relative error (%) due to the adsorption/ desorption equilibrium	
P introduced (a)	0.13	0.13	10		
P equilibrium (b)	0.105	0.0955	60	**10**	Sticking and outgassing of the near pure gas

Addition of 1atm. Of air (c)		0.145	80	**52**	Modification of the adsorption-desorption equilibrium of the active gas due to the large amount of the collision of the added air.
20 min after the addition of the air (d)		0.12	100	**26**	Reaching a new equilibrium
P equilibrium		<0.1	160	**Few %**	The new steady state is almost reached

Table 6: Possible Relative error (%) due to the adsorption/ desorption equilibrium, GM means gauge measurement, ISM stands for "in situ measurements".

Conclusion

In this article, we have accurately (9%) measured the room temperature absorption cross section of 2-EHN, the most used cetane improver, between 850 and 3000 cm^{-1}, using a FT-IR spectrometer. The results are presented in a 2 columns file containing the absorption cross section as a function of wavenumber. This formatting is directly applicable for measurements at a single wavenumber or the complete set can be integrated into a radiative transfer code.

The main bands have been attributed, thanks to DFT calculations. Geometry optimizations also show the complexity of this flexible molecule, leading to almost iso-energetic conformers with slightly different vibrational spectra.

The co-existence of all these isomers experimentally leads to particularly broad and complex absorption bands with shoulders.

Two approaches based on chemometrics and spectral analysis were used to analyze the cross-section in order to set up a procedure for the accurate quantification of this molecule. The chemometric approach allows for an analysis based on several characteristic bands, which should provide a more robust quantification of 2-EHN in a complex mixture.

We use the absorption cross section to estimate the adsorption processes of 2-EHN molecules on the walls of a stainless steel cell. The perturbation induced by the addition of 1 bar of dry air in the sample was further studied. This approach allows to follow the on-line evolution of the 2-EHN partial pressure

resulting from different adsorption-desorption equilibrium. Indeed, a measurement performed without taking these adsorption/desorption processes into account could easily lead to a 52 % error in the determination of the partial pressure.

Acknowledgements

References

[1] Ickes, A. M., Bohac, S. V., & Assanis, D. N. (2009). Effect of 2-ethylhexyl nitrate cetane improver on NO x emissions from premixed low-temperature diesel combustion. Energy & Fuels, 23(10), 4943-4948.

[2] Qian, W., Huang, H., Pan, M., Huang, R., Tong, C., Guo, X., & Yin, J. (2020). Effects of 2-ethylhexyl nitrate and post-injection strategy on combustion and emission characterizes in a dimethyl carbonate/diesel blending engine. Fuel, 263, 116687.

[3] Kuszewski, H. (2018). Effect of adding 2-ethylhexyl nitrate cetane improver on the autoignition properties of ethanol–diesel fuel blend–Investigation at various ambient gas temperatures. Fuel, 224, 57-67.

[4] Kuszewski, H. (2018). Effect of adding 2-ethylhexyl nitrate cetane improver on the autoignition properties of ethanol–diesel fuel blend–Investigation at various ambient gas temperatures. Fuel, 224, 57-67.

[5] PhD-Thesis, Elodie Nicolau, Biodégradtion du 2-éthylhexyl nitrate par Mycobacterium austroafricanum IFP 2173 : de l'élucidation de la voie de dégradation aux enzymes impliquées. http://hal.archives-ouvertes.fr/docs/00/33/49/74/PDF/these271008-en_ligne.pdf

[6] Roberts, J.M., 1990. The atmospheric chemistry of organic nitrates. Atmospheric Environment Part A e General Topics 24, 243e287

[7] Atkinson, R., 1997. Gas-phase tropospheric chemistry of volatile organic compounds: 1. Alkanes and alkenes. Journal of Physical and Chemical Reference Data 26, 215e290.

[8] Solano-Serena, F., Nicolau, E., Favreau, G., Jouanneau, Y., & Marchal, R. (2009). Biodegradability of 2-ethylhexyl nitrate (2-EHN), a cetane improver of diesel oil. Biodegradation, 20(1), 85-94.

[9] Bornemann, H., Scheidt, F., & Sander, W. (2002). Thermal decomposition of 2-ethylhexyl nitrate (2-EHN). International journal of chemical kinetics, 34(1), 34-38.

[10] Insausti, M., & Fernández Band, B. S. (2016). Fast Determination of 2-Ethylhexyl Nitrate Diesel/Biodiesel Blends by Distillation Curves and Chemometrics. Energy & Fuels, 30(7), 5341-5345.

[11] Oung, R., Morin, A. G., & Foucher, F. (2020). Study on the Effects on Diesel LTC Combustion of 2-EHN as Cetane Improver (No. 2020-01-1125). SAE Technical Paper.

[12] Zanão, L. R., Diniz Brito dos Santos, B. C., Sequinel, R., Flumignan, D. L., & De Oliveira, J. E. (2018). Prediction of Relative Density, Distillation Temperatures, Flash Point, and Cetane Number of S500 Diesel Oil Using Multivariate Calibration of Gas Chromatographic Profiles. Energy & Fuels, 32(8), 8108-8114.

[13] Vrtiška, D., & Šimáček, P. (2018). Prediction of 2-EHN content in diesel/biodiesel blends using FTIR and chemometrics. Talanta, 178, 987-991.

[14] Insausti, M., & Fernández Band, B. S. (2014). Determination of 2-ethylhexyl Nitrate in Diesel Oil Using a Single Excitation Emission Fluorescence Spectra (EEF) and Chemometrics Analysis.

[15] Insausti, M., & Band, B. S. F. (2015). Single excitation–emission fluorescence spectrum (EEF) for determination of cetane improver in diesel fuel. Spectrochimica Acta Part A: Molecular and Biomolecular Spectroscopy, 140, 416-420.

 [16] Jacquemart, D., Guinet, M. (2016). Line parameters measurements and modeling for nu(6) band of CH3F: Generation of a complete line list for atmospheric database. Journal of quantitative spectroscopy and radiative transfer, 185, 58-69.

[17] Gaussian 09, Revision D.01, M. J. Frisch, G. W. Trucks, H. B. Schlegel, G. E. Scuseria, M. A. Robb, J. R. Cheeseman, G. Scalmani, V. Barone, G. A. Petersson, H. Nakatsuji, X. Li, M. Caricato, A. Marenich, J. Bloino, B. G. Janesko, R. Gomperts, B. Mennucci, H. P. Hratchian, J. V. Ortiz, A. F. Izmaylov, J. L. Sonnenberg, D. Williams-Young, F. Ding, F. Lipparini, F. Egidi, J. Goings, B. Peng, A. Petrone, T. Henderson, D. Ranasinghe, V. G. Zakrzewski, J. Gao, N. Rega, G. Zheng, W. Liang, M. Hada, M. Ehara, K. Toyota, R. Fukuda, J. Hasegawa, M. Ishida, T. Nakajima, Y. Honda, O. Kitao, H. Nakai, T. Vreven, K. Throssell, J. A. Montgomery, Jr., J. E. Peralta, F. Ogliaro, M. Bearpark, J. J. Heyd, E. Brothers, K. N. Kudin, V. N. Staroverov, T. Keith, R. Kobayashi, J. Normand, K. Raghavachari, A. Rendell, J. C. Burant, S. S. Iyengar, J. Tomasi, M. Cossi, J. M. Millam, M. Klene, C. Adamo, R. Cammi, J. W. Ochterski, R. L. Martin, K. Morokuma, O. Farkas, J. B. Foresman, and D. J. Fox, Gaussian, Inc., Wallingford CT, 2016.

[18] Rossard, V., Boulet, J. C., Gogé, F., Latrille, E., Roger, J.-M. (2016). ChemFlow, chemometrics using Galaxy. Presented at Galaxy Community Conference - GCC2016, Bloomington, USA (2016-06-24 - 2016-07-29). https://doi.org/10.7490/f1000research.1112573.1

 [19] C. Clerbaux, A. Boynard, L. Clarisse, M. George, J. Hadji-Lazaro, H. Herbin, D. Hurtmans, M. Pommier, A. Razavi, S. Turquety, C. Wespes, and P.-F. Coheur, "Monitoring of atmospheric composition using the thermal infrared iasi/metop sounder", Atmosphere Chemistry and Physics, vol. 9(16), 2009, pp. 6041-6054

[20] Ramchani, AB., Jacquemart, D., Soulard, P., Guinet, M. (2017). Measurements and modeling of N-2 broadening coefficients for the nu(6) band of CH3F, comparison with CH3Cl and CH3Br molecules. Journal of quantitative spectroscopy and radiative transfer, 203, 480-489.

[21] Raddaoui, E., Soulard, P., Guinet, M., Aroui, H., Jacquemart, D., Measurements and modeling of air broadening coefficients for the nu(6) band of CH3I. Journal of quantitative spectroscopy and radiative transfer, 246, 106934.

Supplementary Information

(The spectrum will be added as a .dat file. The fortran file will also be added)

Main vibrational frequencies of the two most stable isomers with their attributions

A

1785.44	428.0375	N-O twisting
925.7941	172.9887	N-O stretching linked to the carbon chain
930.886	131.8025	N-O stretching linked to the carbon chain
1368.317	125.9247	H methyl wagging, N-O sym stretching
1433.583	108.1485	H methyl wagging, N-O sym stretching
1385.218	60.6929	H methyl wagging, N-O sym stretching
3101.448	56.2806	C-H stretching asymm
1049.763	13.1103	C-O stretching asymm
1036.122	56.5542	C-O stretching symm
3133.563	47.9049	C-H stretching asymm
1068.163	21.0466	C-O stretching asymm
1068.045	17.0478	C-O stretching asymm
3051.905	46.2258	C-H stretching symm
3048.018	41.9273	C-H stretching symm
3055.14	41.5464	C-H stretching symm
1348.622	41.1347	H methyl twisting and wagging, N-O sym stretching
3141.323	33.9922	C-H stretching asymm
3062.863	31.8938	C-H stretching symm
3135.978	29.7327	C-H stretching asymm
3141.583	26.8459	C-H stretching asymm
3095.73	25.7462	C-H stretching asymm
3169.423	16.3973	
3077.843	18.8254	C-H stretching symm
1325.716	18.753	H methyl twisting and wagging
792.9368	11.8722	NO3 umbrella mode
776.523	10.9603	CH2-CH3 twisting

1501.048	10.1029	C-H twisting

B

1784.551	429.0552	N-O twisting
934.154	239.5948	N-O stretching linked to the carbon chain
949.1944	60.5901	overall vibration
1366.278	110.8232	H methyl wagging, N-O sym stretching
1432.367	109.8515	H methyl wagging
1385.447	63.0674	H methyl wagging, N-O sym stretching
3054.488	62.1802	C-H mouvement d'ensemble
1043.444	57.8258	C-O stretching symm
3132.099	52.3671	C-H stretching asymm
3139.785	33.8518	C-H stretching asymm
1061.449	41.4644	C-O stretching asymm
3048.427	41.1771	C-H stretching symm
3140.837	38.416	C-H stretching asymm
3105.188	35.9236	C-H stretching asym
1338.402	33.6815	H methyl wagging, N-O sym stretching
3060.944	31.9234	stretching symm
3143.93	31.7857	C-H stretching asym des CH2
3053.644	31.2232	stretching symm
3108.678	20.5613	C-H stretching asym
3154.796	18.9443	C-H stretching asym
1416.116	15.0981	methyls vibration, overall vibration
1328.826	14.2712	C-H vibration d'ensemble
1395.945	12.4733	
3085.161	13.7066	C-H stretching symm
1500.955	11.5562	CH3 rotation
792.6936	11.5526	NO3 umbrella mode
778.6432	8.2278	
1509.208	10.994	C-H stretching symm
1502.091	8.6898	

Energetic, geometric, and vibrational characteristics of all identified isomers

A

Sum of electronic and zero-point Energies=   -594.494973

```
N    -3.376696  -0.616721   0.135028
O    -3.328060  -1.722019  -0.352101
O    -4.332322   0.001798   0.520064
O    -2.184392   0.071497   0.289701
C    -1.020826  -0.648306  -0.162272
C     0.197779   0.233248   0.071717
C     1.437666  -0.584012  -0.329646
C     0.127915   1.570265  -0.686925
C     2.744407  -0.063444   0.262803
C    -0.603533   2.696051   0.038689
C     3.965827  -0.857320  -0.191654
C     5.267018  -0.349303   0.417904
H    -1.140328  -0.885664  -1.225577
H    -0.948972  -1.585373   0.398571
H     0.259051   0.439149   1.150846
H     1.511929  -0.603428  -1.426991
H     1.310889  -1.629733  -0.015306
H    -0.334053   1.394428  -1.668915
H     1.151809   1.902100  -0.896921
H     2.678761  -0.094981   1.359844
H     2.887148   0.992999  -0.002182
H    -0.577744   3.617025  -0.552880
H    -0.127575   2.910064   1.002589
H    -1.649599   2.447662   0.232041
H     4.033549  -0.819648  -1.287442
H     3.826961  -1.915817   0.067639
H     6.126045  -0.934670   0.074942
H     5.240856  -0.407478   1.512004
H     5.448842   0.697121   0.147529
```

31.33 (1.0797) 47.7728 (0.1329) 53.617 (0.4399) 62.147 (0.2531) 637.717 (2.6956) 83.5157 (0.2122) 410.42 (0.1336) 490.1574 (0.4658) 527.8026 (0.6946) 729.0058 (3.8554) 732.8997 (3.2043) 776.523 (10.9603) 786.1348 (4.9281) 792.9368 (11.8722) 846.179 (0.6286) 914.285 (1.722) 925.7941 (172.9887) 93.3645 (0.4894) 930.886 (131.8025) 977.5163 (5.4331) 1011.0463 (2.2146) 1036.122 (56.5542) 1049.763 (13.1103) 1068.0458 (17.0478) 1068.163 (21.0466) 1095.1983 (6.1271) 1109.2929

(4.4382) 1158.871 (2.3305) 1176.8367 (1.4972) 1189.6918 (0.6527) 1236.202 (0.3191) 1256.9073

(0.5426) 1271.3672 (0.3973) 1305.161 (0.2863) 1310.7167 (1.517) 1325.7165 (18.753) 1331.413

(0.3329) 1348.6221 (41.1347) 1368.3175 (125.9247) 1385.218 (60.6929) 1400.9225 (0.995) 1415.5296

(5.8886) 1417.139 (1.8747) 1419.554 (7.2836) 1433.5832 (108.1485) 144.497 (0.1234) 1483.635

(1.8565) 1487.8029 (0.6806) 1489.566 (1.5678) 1498.206 (2.8899) 1499.2083 (9.383) 1501.0485

(10.1029) 1508.817 (3.6323) 1510.1446 (7.1821) 1512.2611 (8.6456) 160.0794 (0.3421) 1785.44

(428.0375) 179.2928 (0.8861) 225.809 (0.4004) 236.8073 (0.442) 247.3003 (0.1444) 266.197 (0.2759)

3032.1377 (7.5387) 3038.5522 (3.8761) 3042.64 (2.0798) 3048.0186 (41.9273) 3051.9059 (46.2258)

3055.14 (41.5464) 3062.8636 (31.8938) 3068.6927 (5.5121) 3077.843 (18.8254) 308.7582 (0.4835)

3080.2812 (2.7618) 3095.7306 (25.7462) 3101.448 (56.2806) 3133.5635 (47.9049) 3135.9781

(29.7327) 3141.323 (33.9922) 3141.5836 (26.8459) 3169.4232 (16.3973) 334.4279 (0.2803)

B

Sum of electronic and zero-point Energies=   -594.496687

N	2.978445	-1.130103	-0.070085
O	3.256329	-2.160979	-0.621547
O	3.652394	-0.457034	0.674777
O	1.698933	-0.687221	-0.355924
C	1.335307	0.549061	0.290923
C	-0.099577	0.846422	-0.119868
C	-1.062436	-0.199475	0.458568
C	-0.465176	2.275324	0.310514
C	-2.440012	-0.224091	-0.198166
C	0.215415	3.384227	-0.486558
C	-3.364202	-1.283778	0.395500
C	-4.736804	-1.316372	-0.265781
H	1.422260	0.425596	1.376332
H	2.031413	1.327897	-0.030580
H	-0.145117	0.794691	-1.218171
H	-1.171197	-0.020524	1.539182
H	-0.612412	-1.194599	0.354251
H	-0.245028	2.393287	1.381388
H	-1.550232	2.392952	0.216162
H	-2.320994	-0.411622	-1.275068
H	-2.926068	0.757297	-0.111410
H	-0.135032	4.367943	-0.158834

```
H     -0.007276    3.292981   -1.555575
H      1.304404    3.377995   -0.373205
H     -2.888106   -2.269368    0.304071
H     -3.478995   -1.100619    1.472641
H     -4.654405   -1.530487   -1.337518
H     -5.250654   -0.353854   -0.160115
H     -5.378008   -2.084872    0.177802
```

37.7606 (0.3517) 43.2831 (0.2473) 43.7817 (0.7851) 63.9145 (0.0869) 68.6074 (0.3064) 381.932

(0.5234) 395.0889 (0.3713) 491.1555 (0.8895) 507.5438 (0.2058) 632.8833 (4.4388) 731.2835 (6.0996)

732.8982 (1.2854) 778.6432 (8.2278) 784.1002 (2.8513) 792.6936 (11.5526) 867.1488 (5.0238)

911.5005 (0.7955) 917.0669 (3.4569) 934.154 (239.5948) 949.1944 (60.5901) 1005.0813 (2.153)

1043.4446 (57.8258) 1051.1523 (4.5453) 1061.449 (41.4644) 1068.1006 (3.5624) 1094.2955 (0.9502)

1103.6392 (1.7617) 1164.9688 (1.5619) 1180.8117 (2.5383) 1186.6172 (0.9909) 119.5392 (0.2396)

1235.5098 (0.882) 1253.6714 (2.2024) 1282.6476 (3.4634) 1290.5735 (1.0372) 1318.5809 (0.4956)

1328.8269 (14.2712) 133.721 (0.0932) 1338.4026 (33.6815) 1343.6752 (7.5567) 1366.2782 (110.8232)

1385.447 (63.0674) 1395.9456 (12.4733) 1416.1165 (15.0981) 1417.1518 (2.5641) 1423.3152 (3.876)

1432.3674 (109.8515) 1483.5371 (2.0965) 1488.1224 (1.0922) 1491.4684 (0.5519) 1498.5179 (2.0973)

1500.955 (11.5562) 1502.091 (8.6898) 1505.8227 (5.9652) 1509.2087 (10.994) 1511.1225 (6.0251)

156.5173 (0.2551) 165.7132 (1.0003) 1784.5519 (429.0552) 216.9998 (0.1958) 236.2038 (0.2186)

249.8445 (0.1117) 264.0217 (0.9608) 3032.3062 (2.6214) 3037.3877 (6.3018) 304.3471 (0.0238)

3043.0359 (0.9983) 3048.427 (41.1771) 3053.6443 (31.2232) 3054.4882 (62.1802) 3060.9446

(31.9234) 3071.1351 (0.9) 3085.1619 (13.7066) 3089.7812 (4.3355) 3105.1886 (35.9236) 3108.6784

(20.5613) 3132.0992 (52.3671) 3139.7853 (33.8518) 3140.8379 (38.416) 3143.9307 (31.7857)

3154.7966 (18.9443)

C

Sum of electronic and zero-point Energies=   -594.492244

```
N      2.756988   -0.880832    0.001843
O      2.606465   -0.918386    1.199370
O      3.297085   -1.678846   -0.715410
O      2.266886    0.214614   -0.698925
C      1.536707    1.198549    0.061489
C      0.038133    1.127442   -0.213829
C     -0.531096   -0.243328    0.167102
```

```
C    -0.636187    2.304802    0.521825
C    -2.015167   -0.434612   -0.131481
C    -1.718783    3.012677   -0.287660
C    -2.501285   -1.849914    0.169271
C    -3.985894   -2.043356   -0.115218
H     1.760887    1.071038    1.123319
H     1.952370    2.151250   -0.280439
H    -0.099300    1.268448   -1.296381
H    -0.350030   -0.418591    1.237561
H     0.027977   -1.020247   -0.371389
H     0.123021    3.049816    0.799150
H    -1.051603    1.943273    1.471743
H    -2.210335   -0.202866   -1.188778
H    -2.612399    0.276785    0.454976
H    -2.170470    3.827647    0.287221
H    -2.519887    2.328989   -0.583240
H    -1.300450    3.445147   -1.203469
H    -2.293928   -2.086746    1.221749
H    -1.916094   -2.566045   -0.423313
H    -4.307097   -3.066042    0.106690
H    -4.216354   -1.844081   -1.168105
H    -4.597291   -1.364570    0.490534
```

41.3396 (1.0291) 45.8885 (0.5028) 54.5754 (0.1444) 79.7009 (0.1547) 82.218 (0.1195) 98.2011 (0.0025) 107.306 (0.0544) 158.778 (0.0903) 194.5604 (0.4499) 226.5527 (0.1447) 247.7389 (0.0589) 264.7896 (0.4388) 301.6883 (0.5732) 355.0431 (0.2823) 391.8192 (2.0096) 402.374 (1.9997) 459.1119 (0.6185) 522.5722 (2.6187) 648.8524 (10.4582) 684.5786 (21.248) 742.2351 (3.5318) 771.271 (5.7025) 783.3358 (8.3835) 791.8518 (2.5866) 849.4547 (1.4214) 893.3798 (126.5382) 912.9384 (23.1619) 925.3158 (61.3047) 961.3402 (38.4826) 1027.5708 (14.6792) 1032.9771 (47.5705) 1052.7333 (44.2584) 1058.3582 (15.2551) 1064.1934 (29.5372) 1094.1471 (0.3091) 1099.6789 (2.6676) 1159.8203 (2.4123) 1173.44 (2.4584) 1193.5214 (0.1609) 1241.8498 (0.3173) 1270.8745 (0.2632) 1288.8738 (1.9783) 1301.216 (1.3163) 1311.1675 (0.8468) 1331.7235 (1.3877) 1341.7445 (8.5573) 1358.0635 (3.6222) 1367.2258 (140.9094) 1388.6567 (10.0569) 1398.8195 (15.7451) 1413.3565 (0.8843) 1417.2276 (4.2947) 1422.7292 (81.0484) 1424.7273 (0.8218) 1480.6593 (7.0888) 1483.5092 (26.1766) 1488.1075 (0.1623) 1494.5434 (3.7552) 1498.3314 (5.3579) 1500.7737 (10.4517) 1502.5923 (3.2351) 1508.3622 (5.7732) 1510.1142 (13.1305) 1789.1236 (423.2035) 3034.0426 (2.9973) 3038.5319 (5.1806) 3041.1969 (19.55) 3045.9286 (10.5356) 3050.0338 (71.1764) 3053.8874 (45.3617) 3061.9665 (32.1796) 3071.2194 (0.5791) 3084.4871 (14.9717) 3088.0193 (1.0284) 3099.4408 (26.232) 3104.0108 (53.1471) 3131.9915 (50.665) 3139.0235 (34.4012) 3140.372 (34.2865) 3153.4544 (27.7451) 3168.6097 (4.1393)

D

Sum of electronic and zero-point Energies=   -594.492557

```
N     3.205677  -0.397868   0.074472
O     3.022177  -0.751132   1.214809
O     4.189721   0.088950  -0.413613
O     2.179955  -0.552038  -0.848826
C     0.927329  -1.068771  -0.353069
C    -0.164048  -0.005111  -0.312558
C    -1.462079  -0.701412   0.127043
C     0.188296   1.186268   0.595581
C    -2.732743   0.069182  -0.220685
C     0.970036   2.306262  -0.087254
C    -4.003889  -0.616458   0.272038
C    -5.272136   0.145042  -0.094529
H     1.091139  -1.511243   0.632390
H     0.673890  -1.862716  -1.062393
H    -0.307095   0.365945  -1.338638
H    -1.421473  -0.877664   1.212175
H    -1.525223  -1.695701  -0.338955
H     0.737709   0.819224   1.472837
H    -0.743385   1.611441   0.987576
H    -2.788310   0.196346  -1.311374
H    -2.687934   1.082682   0.200845
H     1.187441   3.114457   0.618335
H     0.389597   2.734652  -0.912322
H     1.920718   1.964230  -0.505220
H    -3.949403  -0.737097   1.362570
H    -4.051903  -1.632328  -0.143671
H    -6.167651  -0.367293   0.271259
H    -5.370301   0.250910  -1.180954
H    -5.266970   1.152972   0.335867
```

34.0462 (1.0459) 39.7469 (0.7209) 55.2697 (0.5005) 60.6102 (0.1173) 75.4959 (0.0733) 89.4308 (0.1612)

140.7073 (0.076) 152.2197 (0.1202) 186.984 (0.3188) 230.8706 (0.5438) 243.6971 (0.0061) 267.6778 (0.6257)

300.8447 (0.425) 306.9383 (0.0433) 375.3845 (2.1177) 415.7839 (1.1963) 471.8774 (2.13) 527.867 (1.95)

655.3858 (12.2641) 684.7497 (16.4679) 732.3702 (3.4487) 769.7697 (13.8796) 783.8276 (7.3377) 789.3343

(3.4028) 833.7218 (0.5313) 899.4894 (183.3801) 914.1678 (1.6703) 927.613 (46.6767) 978.0595 (13.11)

998.9115 (4.9871) 1039.2895 (0.597) 1041.9512 (121.1117) 1059.3173 (32.0496) 1066.3584 (1.3167) 1094.211

(2.8343) 1108.8954 (12.8656) 1151.6978 (0.9243) 1182.3902 (1.4097) 1189.4775 (0.617) 1237.7663 (0.1003)

1265.5977 (0.1438) 1281.9998 (1.0467) 1308.3526 (0.3852) 1319.2593 (3.4336) 1327.481 (9.119) 1332.326

(3.1448) 1353.3762 (16.2484) 1370.6496 (112.0738) 1384.524 (52.0139) 1405.212 (0.0683) 1416.2245 (5.0136)

1417.2627 (1.4065) 1422.1955 (8.1767) 1426.3178 (65.3305) 1477.9387 (11.6167) 1487.2816 (4.7468)

1488.6804 (5.8064) 1495.8542 (9.1344) 1498.9941 (9.0504) 1499.9602 (9.0586) 1500.8677 (10.3845) 1509.1513

(11.6812) 1511.2588 (8.9049) 1787.0253 (404.131) 3029.2753 (12.2392) 3037.8036 (1.7421) 3042.1236 (3.4322)

3047.7143 (66.8106) 3054.9309 (40.2853) 3059.612 (19.5037) 3063.566 (30.1643) 3066.9852 (10.4039)

3078.529 (3.6332) 3096.7726 (10.8215) 3099.2275 (47.3738) 3101.4951 (40.3031) 3133.3142 (49.5831)

3138.7886 (31.5489) 3141.0867 (33.8971) 3159.6343 (22.2767) 3167.8719 (3.8632)

E

Sum of electronic and zero-point Energies=　　　-594.494373

N	-3.082320	-0.693639	0.278399
O	-3.632966	-0.900423	-0.777952
O	-3.488761	-0.877206	1.394552
O	-1.801761	-0.170136	0.245005
C	-1.286216	0.059690	-1.083156
C	0.137937	0.584171	-0.954730
C	1.045161	-0.421205	-0.234841
C	0.220637	2.021998	-0.410865
C	2.529430	-0.071532	-0.284146
C	0.004385	2.201413	1.089544
C	3.416009	-1.148532	0.334950
C	4.898334	-0.796703	0.296705
H	-1.308270	-0.887272	-1.632205
H	-1.935959	0.777260	-1.594820
H	0.475562	0.633912	-2.002555
H	0.899719	-1.409366	-0.694790
H	0.725240	-0.527564	0.809043
H	-0.505446	2.637087	-0.959587
H	1.205188	2.425875	-0.676872
H	2.709731	0.879133	0.235960
H	2.833655	0.090672	-1.329114
H	0.088047	3.259602	1.357470
H	0.754008	1.658013	1.674362
H	-0.979701	1.849393	1.408897
H	3.249602	-2.099284	-0.189719
H	3.104608	-1.317749	1.374718
H	5.510092	-1.586456	0.744393
H	5.099484	0.130445	0.845586
H	5.244522	-0.651903	-0.733174

38.6418 (1.1618) 48.0683 (0.1677) 57.9676 (0.2432) 67.5058 (0.0842) 96.2403 (0.2304) 124.8756 (0.0724)
132.5039 (0.1441) 165.2526 (0.5965) 175.1819 (0.1412) 240.2529 (0.5258) 244.0231 (0.5654) 247.0508 (0.0975)
270.8984 (0.1513) 317.7024 (0.0565) 350.9379 (0.3307) 446.8296 (0.3557) 491.7455 (0.394) 573.4875 (0.807)
635.4039 (6.7093) 733.6865 (2.7788) 745.1855 (1.6041) 781.3619 (2.9104) 792.2909 (9.6518) 801.9505 (7.4957)
818.2983 (1.9303) 914.5382 (9.8644) 928.3712 (155.8986) 934.7236 (3.5013) 942.921 (152.5883) 1000.989
(3.632) 1032.62 (26.3854) 1036.2509 (34.6372) 1048.8568 (7.9283) 1062.6426 (6.4793) 1094.792 (0.5837)
1110.0382 (5.7713) 1143.1151 (8.8302) 1174.7573 (0.8651) 1194.3075 (1.3952) 1237.8945 (0.5177) 1261.7014
(1.0999) 1279.7078 (2.2415) 1298.0237 (0.4656) 1317.0511 (0.5679) 1332.2762 (2.9409) 1343.1924 (4.5242)

1355.5341 (199.2678) 1374.2177 (5.3843) 1383.1402 (26.5912) 1394.3997 (0.9875) 1416.3469 (0.8751) 1418.427 (35.1709) 1423.1942 (10.6995) 1431.6343 (104.2792) 1485.48 (1.0521) 1487.6498 (1.7863) 1492.261 (4.9788) 1496.9759 (4.9572) 1500.8896 (10.2934) 1505.2529 (12.0037) 1507.5983 (12.1526) 1509.0811 (3.0179) 1515.4104 (0.3247) 1784.0368 (416.2436) 3024.5973 (11.5242) 3032.1292 (8.4868) 3042.7099 (4.1424) 3047.8844 (67.2908) 3053.8713 (36.055) 3054.8783 (35.9453) 3068.4193 (22.1515) 3071.5114 (6.5475) 3082.6767 (16.6877) 3090.2327 (9.2658) 3095.7298 (26.3666) 3108.3371 (45.2789) 3132.1697 (52.3551) 3140.2088 (37.9338) 3140.9798 (16.9128) 3142.7024 (31.9063) 3164.8166 (21.5254)